Zebrafish Rif1 Impacts Zygotic Genome Activation, Replication Timing, and Sex Determination

Emily A. Masser[1,2], Tyler D. Noble[1,2], Joseph C. Siefert[1,2], Duane Goins[2], Courtney G. Sansam[2], Christopher L. Sansam[1,2]

[1] University of Oklahoma Health Sciences Center, Department of Cell Biology, Oklahoma City, OK
[2] Oklahoma Medical Research Foundation, Cell Cycle and Cancer Biology Research Program, Oklahoma City, OK

ORCID IDs
Emily A. Masser: https://orcid.org/0000-0002-7934-7175
Tyler D. Noble: https://orcid.org/0000-0002-6073-7691
Joseph C. Siefert: https://orcid.org/0000-0001-5584-8672
Duane Goins: https://orcid.org/0000-0003-3154-9007
Courtney G. Sansam: https://orcid.org/0000-0002-0253-8643
Christopher L. Sansam: https://orcid.org/0000-0002-0545-2693

ABSTRACT

Deregulated DNA replication causes human developmental disorders and cancer, but we know little about how DNA replication is coordinated with changes in transcription and chromatin structure. The initiation of replication forks follows a spatiotemporal pattern called the replication timing program. We have developed the zebrafish into a model system to study the mechanisms by which the replication timing program changes during the extensive changes in the cell cycle, transcription, chromatin organization, and nuclear structure that occur during development. Our previous studies identified changes in DNA replication timing patterns occurring from the onset of zygotic transcription through gastrulation in zebrafish embryos. Rif1 is required for DNA replication timing in a wide range of eukaryotes. The broader role of Rif1 in establishing the replication timing program and chromatin structure during early vertebrate development remains unknown. We have generated Rif1 mutant zebrafish and have performed RNA sequencing and whole-genome replication timing analyses on multiple developmental stages. Rif1 mutants were viable but had a defect in female sex determination. Surprisingly, Rif1 loss predominantly affected DNA replication timing after gastrulation, while its impacts on transcription were more substantial during zygotic genome activation. Our results indicate that Rif1 has distinct roles in DNA replication and transcription control that manifest at different stages of development.

INTRODUCTION

The initiation of DNA replication follows a pattern where different genomic regions replicate at distinct times throughout S-phase. This temporal pattern is known as the replication-timing program [5]. Replication timing (RT) correlates with chromatin organization and gene activity [6]. In multicellular organisms, early replication often correlates with active transcription; whereas, late replication frequently coincides with transcriptionally silent genes [7-10]. In mammals, pluripotent cells exhibit a replication-timing pattern that changes with cellular differentiation; in addition, the switch in RT is related to changes in epigenetic modifications, transcriptional activity and the three-dimensional (3D) organization of chromatin [5-7, 11, 12]. The causal relationships between DNA replication and developmental changes, such as transcription, chromatin structure and 3D chromatin organization have been unclear.

The Rif1 (Rap1-interacting factor 1) protein is of particular interest because it has been implicated in the regulation of transcription, chromatin structure, 3D chromatin organization, DNA repair, and DNA replication timing. In fact, Rif1 is the single factor known to influence RT in all eukaryotes [5, 13-16]. Through conserved motifs, Rif1 has been shown to interact physically with the PP1 phosphatase [15, 17-20]. Rif1 controls RT by bringing PP1 to late-replicating regions of the genome, thereby causing de-phosphorylation of DNA replication factors during early S-phase and delaying initiation [15-19, 21, 22].

Our understanding of how Rif1 affects RT during embryonic development is incomplete. RT is developmentally regulated through Rif1 in *D. melanogaster* [23]. In early fly embryos, Rif1-activation initiates late replication of satellite repeats and causes the first lengthening of the cell cycle [23]. In Xenopus laevis, Rif1 knockdown accelerates early embryonic cell cycles and disrupts RT patterns in retinal progenitor cells [24]. Loss of Rif1 in mice is embryonic lethal with partial penetrance [25-28]. Cell lines derived from Rif1 mutant mice display altered RT profiles, but the extent to which RT is disrupted in the developing embryo has not been shown. Although Rif1 loss causes RT changes in cell lines from a wide range of species, it is unknown whether

65 Rif1 plays roles in the establishment or change of the RT program during vertebrate
66 embryogenesis.
67 We have developed the zebrafish into a model system to study how modifications in RT
68 coincide with extensive changes in cell cycle and transcription that occur in the developing
69 embryo. The earliest stages of zebrafish development have been extensively studied, so it is
70 possible to collect large numbers of synchronously developing embryos at developmental time
71 points when cells are known to be pluripotent, specified or committed to particular cell fates [29].
72 As a result, it is feasible to study how changes in RT accompany developmentally regulated
73 changes during cellular differentiation in vertebrates. We previously mapped RT at various
74 stages of early wild-type zebrafish development [30]. We revealed that a weak RT pattern
75 present at the onset of zygotic transcription becomes progressively more defined as the fish
76 develop. In addition, during gastrulation, large genomic domains switch from early-to-late
77 replication in the embryo. Finally, we observed that changes in epigenetic modifications involved
78 in enhancer activity correlate with developmental changes in RT [30].
79 To reveal the function of Rif1 in gene expression and RT during vertebrate development,
80 we have generated Rif1 mutant zebrafish, and we have performed RNA sequencing and whole-
81 genome RT analyses before the first major wave of zygotic transcription and before and after
82 gastrulation. We found that Rif1 is not essential for embryonic development, but its loss impairs
83 female sex determination. Although the Rif1 mutants had altered RT at each stage, the effects
84 of Rif1 loss on RT were minor compared to changes that naturally occur during development.
85 DNA replication timing was most affected by Rif1 loss after gastrulation, while transcription was
86 most affected early in development. Rif1 was required for normal expression of genes during
87 the first wave of zygotic genome activation. Our results indicate that in zebrafish, Rif1 has
88 distinct roles in DNA replication and transcription control that manifest at different stages of
89 development.
90

91 **RESULTS**

92 **Generation of a Rif1 loss zebrafish model**

93 The zebrafish genome has a single copy of the *rif1* gene on chromosome 9 (GRCz11
94 22,780,901-22,802,172). Similar to other vertebrates, the *zrif1* gene encodes a 2,347 amino
95 acid protein with heat repeats and PP1 phosphatase interaction sequences (Fig. 1B)[31]. To
96 determine the effects of Rif1 loss-of-function in the zebrafish, we mutated the gene using a
97 transcription activator-like effector nuclease targeting exon 8 (TALEN; Fig. 1A). Frameshift
98 mutations in exon eight would likely induce nonsense-mediated decay (NMD) of the mutant
99 mRNA. If expressed, the mutant allele would produce a protein ending within the sequence
100 encoding the heat repeats (Fig. 1A). We selected a stable line (*rif1*^{omf201}) with a seven base-pair
101 frameshift mutation for further analysis (Fig. 1A).

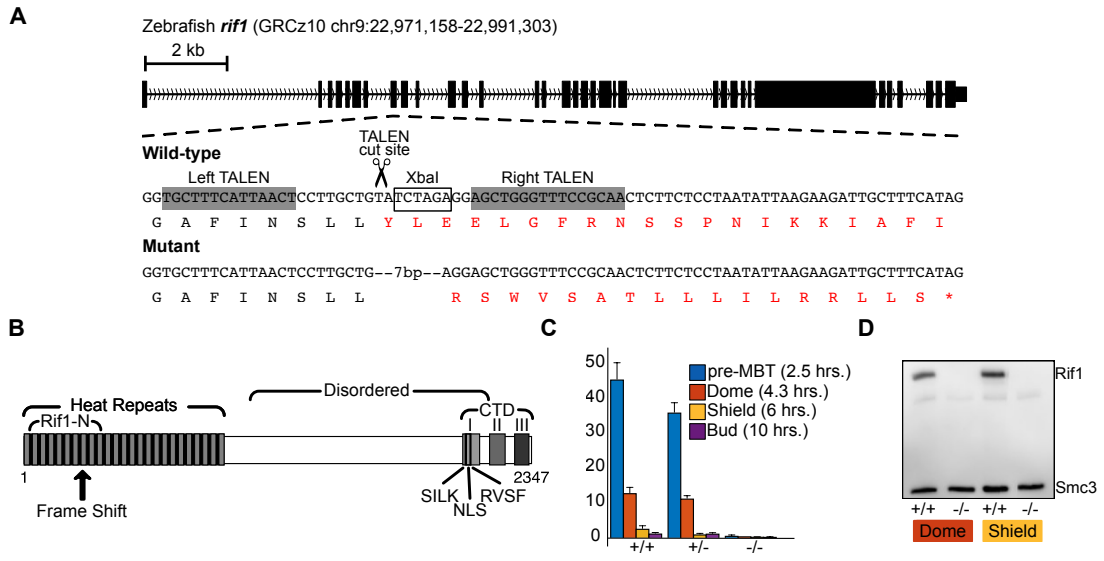

Fig. 1. A TALEN-induced mutation abrogates *rif1* expression in zebrafish. (A) Schematic illustration of the TALEN mutation in exon 8 of the zebrafish *rif1* gene. The DNA and protein sequences at the TALEN site are shown for the wild-type and a 7 bp deletion mutant. The deletion causes a frame shift and introduces a premature termination codon. The affected amino acids are in red. (B) Diagram of the *rif1* protein. The 7 bp frame shift mutation occurs in the conserved *rif1* N-terminal domain (Rif1-N), causing truncation of the Heat repeats and loss of the nuclear localization signal (NLS) and the PP1 phosphatase SILK and RVSF interaction motifs of the C-terminal domain (CTD). (C) Expression levels of *rif1* measured by quantitative RT-PCR analysis at pre-MBT (2.5 hours), dome (4.3 hours), shield (6 hours) and bud (10 hours) in wild-type (+/+), heterozygous (+/-) and homozygous (-/-) *rif1* zebrafish. Error bars represent standard deviation of the mean. (D) Rif1 and Smc3 protein expression levels were analyzed by immunoblotting at dome and shield in wild-type (+/+) and homozygous (-/-) *rif1* zebrafish.

102 We first tested whether zygotic *rif1*^{omf201} mutants developed normally and survived to
103 sexual maturity. Most offspring from *rif1*$^{omf201/+}$ crosses hatched and began free feeding by five
104 days post-fertilization (dpf; data not shown). Therefore, we generated clutches of *rif1*$^{+/+}$,
105 *rif1*$^{omf201/+}$, or *rif1*$^{omf201/omf201}$ embryos spawning F2 mutant and wild-type fish. We then collected
106 embryos of each genotype at 2.5, 4.3, 6, and 10 hours post-fertilization (hpf) and measured *rif1*
107 mRNA by quantitative RT-PCR (Fig. 1C). These developmental time points span the start of
108 zygotic transcription through gastrulation[32]. Our data revealed that *rif1* expression in wild-type
109 zebrafish embryos is developmentally regulated, with the highest expression level at 2.5 hpf and
110 then a precipitous drop at all stages after that (Fig. 1C). The significance of this change in
111 mRNA expression for development is unknown, but we also found that Rif1 protein also
112 decreases in the embryo over these stages (data not shown). The expression level of *rif1*
113 mRNA in heterozygous and homozygous mutant fish was lower than wild-types at all stages
114 (Fig. 1C). In maternal-zygotic homozygous mutants, *rif1* mRNA was nearly undetectable (Fig.
115 1C). Therefore, we conclude the mutation causes a substantial decrease in *rif1* mRNA.
116 To determine if Rif1 protein levels were also affected by the mutation, we generated a
117 polyclonal antibody against the N-terminus of the protein. The antibody's antigen included the
118 portion of the truncated protein that the mutant allele would express (Fig. 1A, B). We did not
119 detect any residual full-length Rif1 protein on immunoblots of nuclear lysates from maternal-
120 zygotic homozygous mutants (Fig. 1D). Furthermore, we have not found evidence on the
121 immunoblots that the *rif1*^{omf201} mutants express truncated Rif1 protein (Fig. 1D). Altogether,
122 these data suggest that the *rif1*^{omf201} mutation eliminates Rif1 protein expression in the embryo.
123
124 **Rif1 is not essential in zebrafish but its loss affects early development and sex**
125 **determination**
126 Given that Rif1 loss in mice caused incompletely penetrant embryonic lethality, we
127 decided to track the development and survival of a large cohort of *rif1*^{omf201} mutants [28]. We

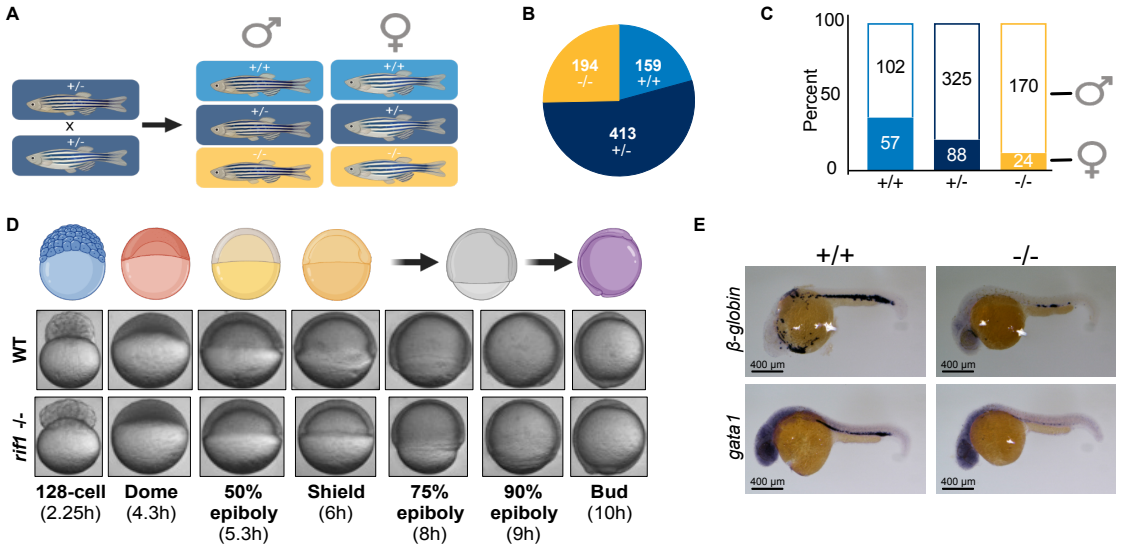

Fig. 2. Loss of *rif1* affects zebrafish sex determination, epiboly, and primitive erythropoiesis. (A) Schematic of the heterozygous *rif1* mutant crosses used to test the essentiality of *rif1.* 766 fish were raised to sexual maturity (3 months) and then genotyped. (B) Quantitation of the genotypes from the heterozygous crosses shows the expected Mendelian ratios. (C) Counts of males and females from the heterozygous crosses shows fewer than expected *rif1* mutant female fish. (D) Time-lapse imaging of wild-type and maternal-zygotic *rif1* -/- early development shows a delay in epiboly completion in the mutants. (E) Expression of *gata1* and *B-globin* at 24 hpf marks primitive erythroid cells. In situ hybridization shows that *gata1* and *B-globin* expression at 24 hpf was decreased in rif1 homozygous mutants, indicating loss of primitive erythroid cells.

raised 766 offspring from *rif1*$^{omf201/+}$ incrosses and counted fish of each genotype when they reached sexual maturity (Fig. 2A, B). Zebrafish sex is determined by poorly defined genetic and environmental factors, so we also counted fish of each gender [33]. Although all genotypes were at their expected mendelian proportions, the number of female heterozygous and homozygous mutants was reduced (Fig. 2B, C). We conclude that although the *rif1*^{omf201} mutation is not zygotic lethal, it does perturb sex determination.

Our qRT-PCR analysis suggested that zebrafish have substantial *rif1* mRNA at pre-MBT (midblastula transition), before full zygotic genome activation (Fig. 1A). Maternally supplied *rif1* mRNA or protein might mask critical functions during early development in zygotic mutants. Therefore, we carefully analyzed the maternal-zygotic *rif1*$^{omf201/omf201}$ mutants, which lack maternally supplied *rif1*, for any overt morphological defects during development. Mutant fish development was delayed by approximately 1 hour at the end of gastrulation (10 hpf; Fig. 2D).

140 Moreover, *rif1*$^{omf201/omf201}$ mutants had fewer circulating blood cells relative to wild types at one

141 dpf. Consistent with the blood cell deficiency, *rif1*$^{omf201/omf201}$ mutants expressed lower levels of

142 hematopoiesis markers (*β-globin* and *gata-1*; Fig. 2E). Despite the delay in early development

143 and the deficiency in primitive hematopoiesis, maternal-zygotic *rif1*$^{omf201/omf201}$ mutants recover

144 and develop to adulthood.

145 **Rif1 loss impairs the establishment of the RT program genome-wide during zebrafish**

146 **development**

147 Given that late replication and S-phase lengthening requires Rif1 in Drosophila, we

148 hypothesized that RT program establishment and change in vertebrates would also depend on

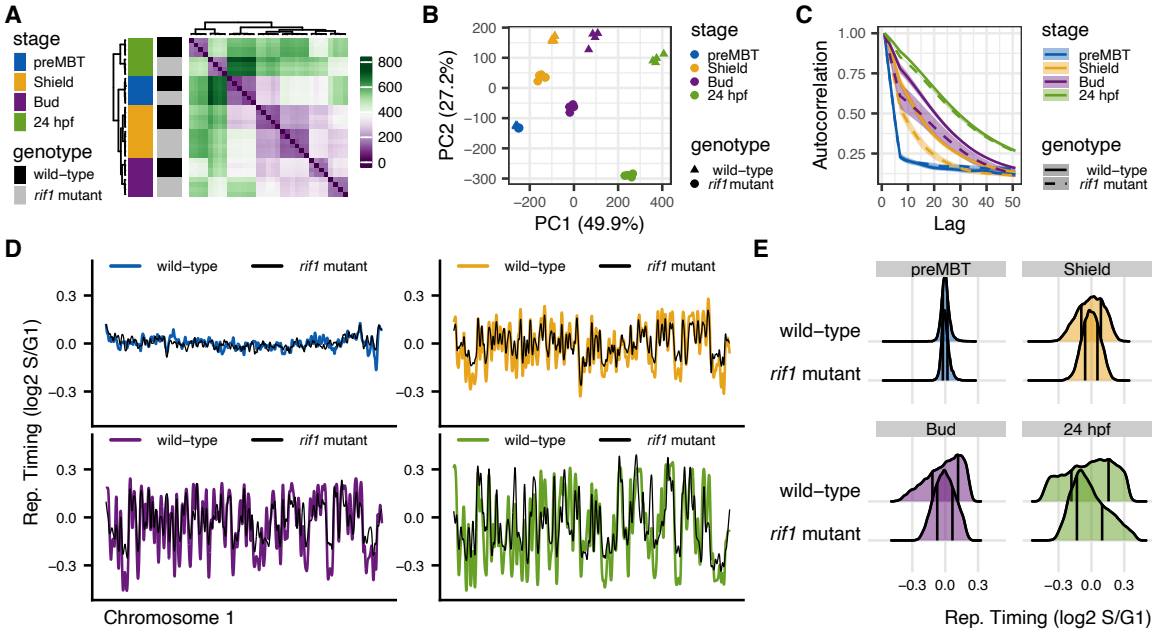

Fig. 3. Rif1 loss reduces the general sharpening of RT patterns that occur during normal zebrafish development. (A) Heat plot and dendograms showing hierarchical clustering of samples based on Euclidean distances calculated with RT values. (B) Principle component analysis reveals that 50% and 27% of variance in RT between samples is due to developmental stage (PC1) and genotype (PC2), respectively. (C) Autocorrelation analysis of RT values shows that RT profiles gradually gain structure during zebrafish development, and Rif1 loss delays that process. (D) Whole chromosome 1 RT profiles are shown for preMBT (top left), shield (top right), bud (bottom left) and 24 hpf (bottom right) stages. The RT profiles gradually develop definition, but Rif1 loss reduces the amplitude of the peaks and valleys. (E) Density plots of genome-wide RT values show a reduced dispersion of values from 0 in the *rif1* mutants compared to wild-types. Vertical black lines within density plots represent 25th and 75th percentiles.

149 Rif1 [23]. We tested this hypothesis by profiling RT in wild-type and *rif1*$^{omf201/omf201}$ mutant
150 zebrafish embryos at multiple stages. We focused on early development because we had
151 previously described changes in RT at multiple timepoints from the 256-cell through gastrulation
152 in zebrafish [30]. We showed that the 256-cell and shield stages in zebrafish are when the RT
153 pattern shifts from being relatively weak to defined [30]. Furthermore, the major wave of zygotic
154 genome activation occurs around the 256-cell stage. Therefore, 256-to-shield is analogous to
155 the stages in Drosophila development when Rif1 promotes the onset of late replication of
156 satellite repeats [23]. We also previously observed that the shield and bud stages are when
157 numerous broad RT changes occur [30]. Therefore, we used whole-genome sequencing to
158 generate RT maps for wild-type and Rif1 mutant zebrafish embryos at 128-cell/pre-MBT (2.25
159 hours), shield (6 hours), bud (10 hours), and 24 hpf.

160 We first assessed overall differences in RT between all genotypes and stages with
161 hierarchical clustering on Euclidean distances between samples (Fig. 3A). Using this approach,
162 we found that samples clustered first by developmental stage and then genotype, demonstrating
163 that the RT changes that occur during zebrafish development are more significant than those
164 caused by Rif1 loss. The Euclidean distances between wild-type and *rif1*$^{omf201/omf201}$ samples
165 were minor at the pre-MBT stage and increased progressively through development, reaching
166 their highest levels at 24 hpf. Importantly, biological replicates of the same developmental stage
167 and genotype were most similar, demonstrating the reproducibility of our RT measurements.

168 The conclusions drawn from the PCA were the same as Euclidean distance analysis
169 (Fig. 3B). All biological replicates clustered together on the PC2 vs. PC1 plot, showing that the
170 data is reproducible. Principal components 1 and 2 described RT differences caused by
171 developmental stage and genotype, respectively. The first principal component, which explained
172 50% of the RT variance, separated samples by developmental stage; the second component,
173 which explained 27% of the variance, separated samples by genotype. Therefore, the
174 developmental stage affected RT more strongly than the genotype. There was no difference

175 between wild-type and *rif1*$^{omf201/omf201}$ samples in the first two principal components at the pre-
176 MBT stage (Fig. 3B; blue points), supporting that Rif1-loss had little effect on RT early in
177 development. As development proceeded, wild-type and *rif1*$^{omf201/omf201}$ mutant samples
178 progressively separated on the second principal component, supporting that RT changes
179 caused by Rif1 loss were more pronounced later in development.

180 We previously showed that the RT pattern in zebrafish embryos gradually gained the
181 hallmark peak-and-valley RT profile structure as development proceeded [30]. We quantitatively
182 assessed the structure of the timing program in wild-type and *rif1*$^{omf201/omf201}$ embryos throughout
183 development by calculating the autocorrelation of timing values along the lengths of the
184 chromosomes at each time point (Fig. 3C). As we described previously, RT value
185 autocorrelation increased between each stage in wild-type embryos [30]. The autocorrelation of
186 *rif1*$^{omf201/omf201}$ RT values also increased during development, but the change lagged behind wild-
187 type. For example, the autocorrelation of *rif1*$^{omf201/omf201}$ RT values at the bud stage was like that
188 of wild-type at shield. The autocorrelation analysis indicated that Rif1 loss delayed the gradual
189 gain in RT profile structure during development.

190 Broad differences in RT were visually evident from plots of normalized (log2 S/G1) RT
191 values at all stages after the MBT (Fig. 3D). At the 128-cell stage (before the MBT), both
192 *rif1*$^{omf201/omf201}$ and wild-type RT profiles were flat compared to those at later stages (Fig. 3D).
193 This was consistent with replication origin firing synchrony at the 128-cell stage in both the wild-
194 type and *rif1* mutants. After the 128-cell stage, the RT profiles of *rif1*$^{omf201/omf201}$ and wild-type
195 embryos developed peak-and-valley structures, but the *rif1*$^{omf201/omf201}$ profiles were less defined
196 (Fig. 3D; compare black lines to colored lines). At each stage after 128-cell, the amplitudes of
197 peaks and valleys appeared lower in the *rif1*$^{omf201/omf201}$ profiles (Fig. 3D). Overall, the RT values
198 (log2 S/G1) in *rif1*$^{omf201/omf201}$ mutants at shield, bud, or 24 hpf were less dispersed from the
199 median than the RT values of wild-type embryos at the same stage (Fig. 3E). Altogether our
200 data show that Rif1 sharpens the genome-wide RT profile during zebrafish development.

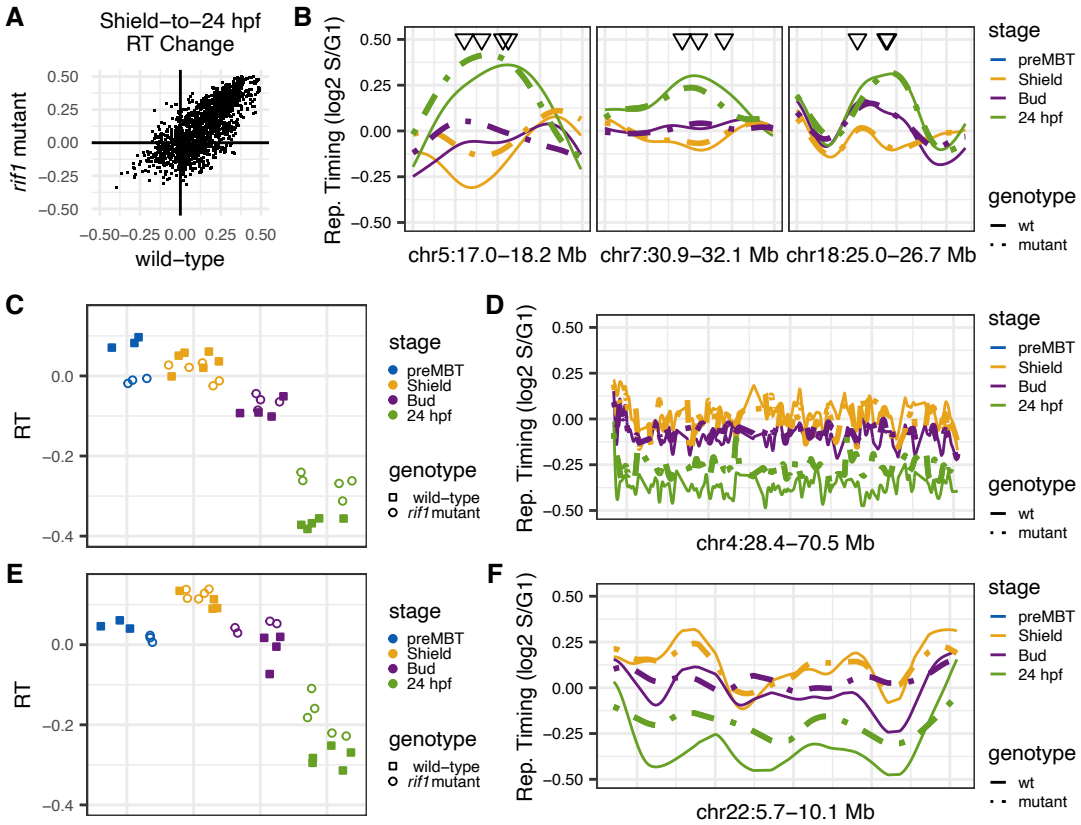

Fig. 4. Rif1 loss does not prevent major changes in RT that occur during early zebrafish development. (A) Scatterplot of changes in RT of 2,498 putative enhancers that are H3K27 acetylated during gastrulation (DARs). A positive shield-to-24 hpf change indicates a switch to earlier replication during gastrulation or segmentation. The majority of acetylated regions switch to earlier replication in both wild-type and *rif1* mutants. (B) RT plotted across three regions with representative DARs. The positions of individual DARs are marked with triangles. (C-F) RT calculated for all of chr4:28,400,000-70,500,000 (C-D) or chr22:5,700,000-10,100,000 (E-F) at each stage and genotype. The broad early-to-late switches in RT during gastrulation occur in the *rif1* mutants.

201

202 **Rif1 is not required for major changes in RT that occur during zebrafish development**

203 We previously identified two significant changes in RT that occur during early zebrafish
204 development [30]. First, genomic domains spanning hundreds of kilobases underwent late-to-
205 early changes in RT. Both coincided with H3K27 acetylation or DNA demethylation at putative
206 enhancers within the domains. Second, ~40 million base-pairs of zebrafish chromosome 4q and
207 a large chromosomal domain on chromosome 22 (5,749,848-10,129,684) both underwent early-

208 to-late RT switches during gastrulation. The mechanisms underlying those changes are
209 unknown.

210 To show whether RT changes that coincide with enhancer activation require Rif1, we
211 calculated RT values at putative enhancers that become acetylated during early zebrafish
212 development (Fig. 3A-B)[34]. The majority (1,768/2,498) of differentially acetylated regions
213 (DARs) that become acetylated between 4.3–24 hpf changed to earlier replicating between the
214 shield (6 hpf) and 24 hpf stages in both wild-type and *rif1*$^{omf201/omf201}$ mutant embryos. Moreover,
215 the shield-to-24 hpf changes in RT for wild-type and *rif1*$^{omf201/omf201}$ DARs were strongly
216 correlated (rs=0.76, p<2.2e-16; Fig. 3A). Therefore, we conclude that Rif1-loss does not
217 generally affect the changes in RT that coincide with enhancer activation during early zebrafish
218 development.

219 To determine whether the early-to-late switches in RT that occur on chromosomes 4 and
220 22 require Rif1, we calculated RT values for Chr4q or Chr22:5,749,848-10,129,684 for both
221 wild-type and *rif1*$^{omf201/omf201}$ embryos at 128-cell, shield, bud, and 24 hpf stages (Fig. 4C-F).
222 Unexpectedly, Chr4q was replicated earlier during S-phase in the *rif1*$^{omf201/omf201}$ embryos than in
223 wild-type embryos at the 128-cell stage, but that difference was minor (Fig. 4C, D). As we
224 previously described, early-to-late RT switches on Chr4q (ANOVA p=7.27e-05) and Chr22
225 (ANOVA p=7.27e-05) occurred between the shield and 24 hpf stages in wild-type embryos (Fig.
226 4C-E). The early-to-late switches at Chr4q (ANOVA p=0.803) and Chr22 (ANOVA p=0.803) also
227 occurred in the *rif1*$^{omf201/omf201}$ mutant embryos (Fig. 4C-E). Although both Chr4q and
228 Chr22:5,749,848-10,129,684 underwent early-to-late switches in the *rif1*$^{omf201/omf201}$ mutant
229 embryos, both were earlier replicating in the mutant compared to wild-types at 24 hpf (Fig. 4C-
230 F). These differences might indicate that those specific timing switches were delayed or
231 incomplete, or it could be due to the genome-wide flattening of the RT profiles. Indeed, when we
232 compared all wild-type and *rif1*$^{omf201/omf201}$ mutant RT values at 24 hpf, we observed that most
233 late-replicating regions were earlier replicating in *rif1*$^{omf201/omf201}$ mutants (Fig. 3D, E). These data

234 have led us to conclude that although Rif1 promotes the establishment of the RT profile

235 genome-wide, it does not generally affect specific RT switches during zebrafish development.

236

237 **Rif1 affects transcription at the earliest stages of zebrafish development**

238 Mouse studies have revealed roles for Rif1 in regulating gene expression and epigenetic

239 marks in embryonic stem cells and cancer cell lines [21, 35, 36]. It has been suggested that Rif1

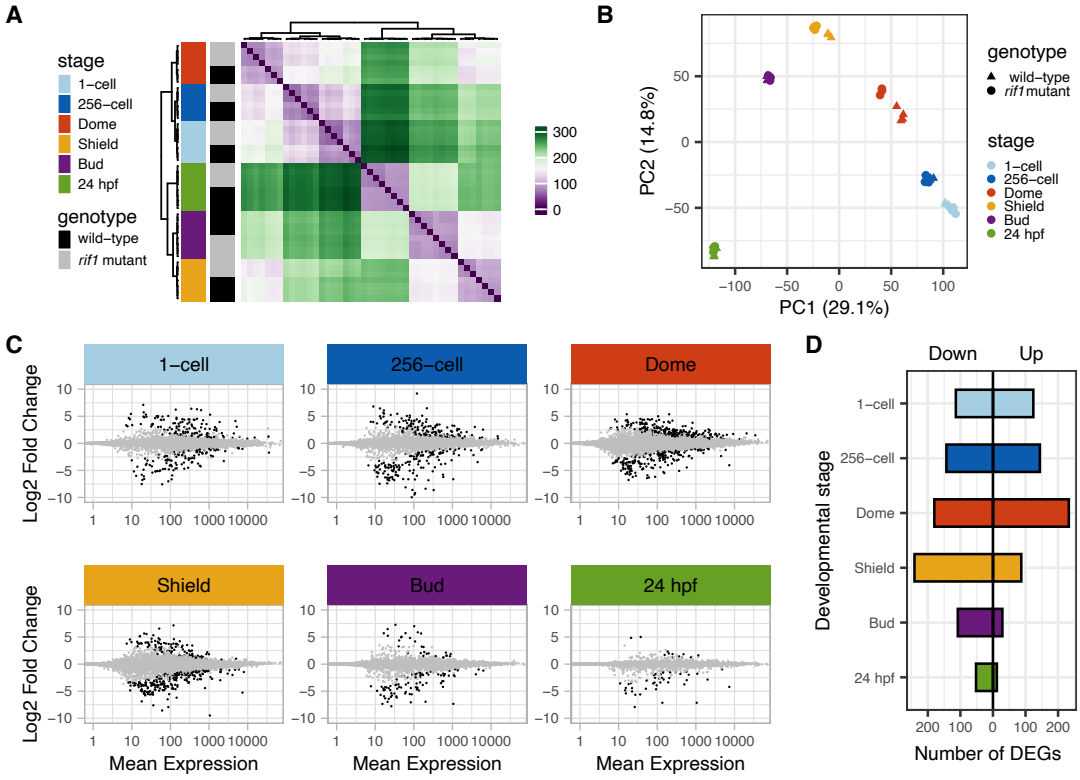

Fig. 5. Rif1 loss affects gene expression preferentially during the earliest stages of zebrafish development. (A) Matrix with colors and dendrograms representing Euclidean distances between 3' mRNA-Seq samples. The order of samples is based on hierarchical clustering and is the same for rows and columns. Each sample's genotype and developmental stage is marked by a color to the left of its row. (B) Principal component analysis (PCA) plot showing clusters of samples based on similarities of 3' mRNA-Seq data. The first two principal components are plotted, which represent 29.1% and 14.8% of the variance. Both the Euclidean distance and PCA analyses show that biological replicates are most similar, followed by samples from the same genotype and then stage. Rif1 mutant and wild-type gene expression differs most at dome and shield stages. (C) Fold-change in expression between *rif1* -/- and wild-type embryos versus normalized mean 3' mRNA-Seq read counts. Black data points represent differentially expressed genes (DEGs) with statistically significant (adjusted Wald test p-value < 0.05; Log2FC > 0.5) changes in expression in the rif1 mutants. (D) Counts of DEGs from C with lower (Down) or higher (Up) expression in *rif1* mutants.

240 affects transcription indirectly, possibly through its RT function [36]. We were particularly
241 interested in whether Rif1 loss would cause transcriptional changes later in development when
242 the RT program is established or in the early embryo, when there is a minimal RT pattern.
243 Therefore, we used 3' end RNA sequencing on maternal-zygotic *rif1*$^{omf201/omf201}$ mutant and wild-
244 type zebrafish embryos at 1-cell (0.2 hours), 256-cell (2.5 hours), dome (4.3 hours), shield (6
245 hours), bud (10 hours) and day 1 (28 hours) (Fig. 5).

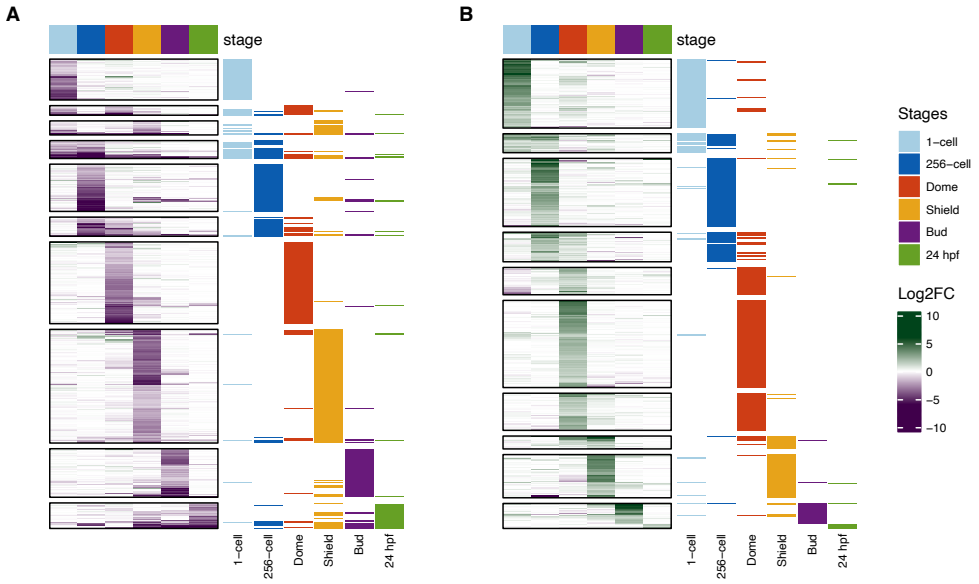

Fig. S5. Most DEGs are at normal levels in maternally-contributed mRNA. Heat plots showing the Log2 fold change in mRNA expression of *rif1* mutants vs wild types for all Down-DEGs (A) or Up-DEGs (B). Genes are displayed in rows and developmental stages are in columns. Rows were split by k-means clustering. Colors in the row annotations to the right of each heat plot denote the stage(s) at which each DEG was identified. The majority of 1-cell DEGs are expressed normally at other stages, and the majority of DEGs at other stages are expressed normally at 1-cell.

246 We determined the overall effects of Rif1 loss on the embryonic transcriptome by
247 analyzing the RNAseq data using principle component analysis (PCA) and hierarchical
248 clustering based on Euclidean distances (Fig. 5A, B). We found that biological replicates were
249 highly similar, and as expected, the transcriptome changed significantly between developmental
250 stages. Rif1 loss impacted the transcriptome at every stage evaluated but not all stages were
251 equally affected, with the most significant effects on gene expression at the dome and shield
252 stages (Fig. 5B). From this point forward, we will refer to differentially expressed genes (DEGs)

253 with higher or lower expression in the maternal-zygotic *rif1*$^{omf201/omf201}$ mutants as Up-DEGs or
254 Down-DEGs, respectively (adjusted Wald test p value < 0.05 and Log2-fold change > 0.5 or < -
255 0.5). The number of Up-DEGs peaked at the dome stage, while the number of Down-DEGs
256 peaked at the shield stage (Fig. 5C-D).
257 Zebrafish contribute most zygotic transcripts maternally, so the differences in transcript
258 abundance in the *rif1*$^{omf201/omf201}$ mutants could be due to changes in the supply or stability of
259 maternal mRNA (Harvey, 2013). We used k-means clustering to categorize all DEGs based on
260 their log-fold change in expression across all stages (Fig. S5A, B). The majority of one-cell
261 DEGs are expressed normally at other stages, and the majority of DEGs at other stages are
262 expressed normally at one-cell (Fig. S5A, B). Therefore, the differential expression of mRNAs at
263 later stages in the *rif1*$^{omf201/omf201}$ mutants is not due to differential maternal contribution.
264
265 **Rif1 broadly suppresses transcription during Zygotic Genome Activation**
266 To learn more about the genes affected by Rif1 loss, we looked at when zebrafish
267 embryos normally express the DEGs. White et al. profiled the zebrafish transcriptome at 18
268 developmental timepoints [1]. We used this dataset to categorize dome DEGs based on when
269 their peak expression occurs in wild-type embryos (Fig. 6A-D). We focused on dome DEGs
270 because they were the most abundant. Dome Up-DEGs are enriched in the Blastula/Gastrula
271 expression cluster (Fig. 6A, C). Since mRNAs that peak at the Blastula and Gastrula stages are
272 likely to be transcribed during the major wave of zygotic genome activation at the MBT, our data
273 suggests Rif1 loss stimulates the transcription of mRNAs at the first major wave of Zygotic
274 Genome Activation (ZGA). Dome Down-DEGs are enriched in the pre-ZGA cluster, which
275 suggests that Rif1 loss also enhances the destruction of maternal mRNAs (Fig. 6B, D). The
276 degradation of many maternal mRNAs in zebrafish is triggered by transcription of the *mir-430*
277 microRNA cluster before the major wave of zygotic transcription [37].

Using complementary approaches, Lee et al. and Heyn et al. defined “first wave” genes that are transcribed immediately upon zygotic genome activation [2, 3]. We used gene set enrichment analysis to determine the extent to which the *rif1*$^{omf201/omf201}$ mutants overexpress first-wave genes (Fig. 6G). At the dome stage, 272 out of 383 first wave genes had a Log2FC > 0 in mutants compared to wild-types. Furthermore, the first wave gene sets were located towards the top of the list of all genes ranked by the dome stage Log2FC (Fig. 4G). Our data indicate that Rif1 loss generally increases the transcription of genes at the ZGA, but by including genes with substantial maternal contribution in our analysis, we might have underestimated that effect. Therefore, we used additional gene sets identified by Harvey et al. as being strictly zygotic or maternal (Fig. 6H)[4]. Like the “first wave” genes, the majority of genes in the zygotic set were expressed

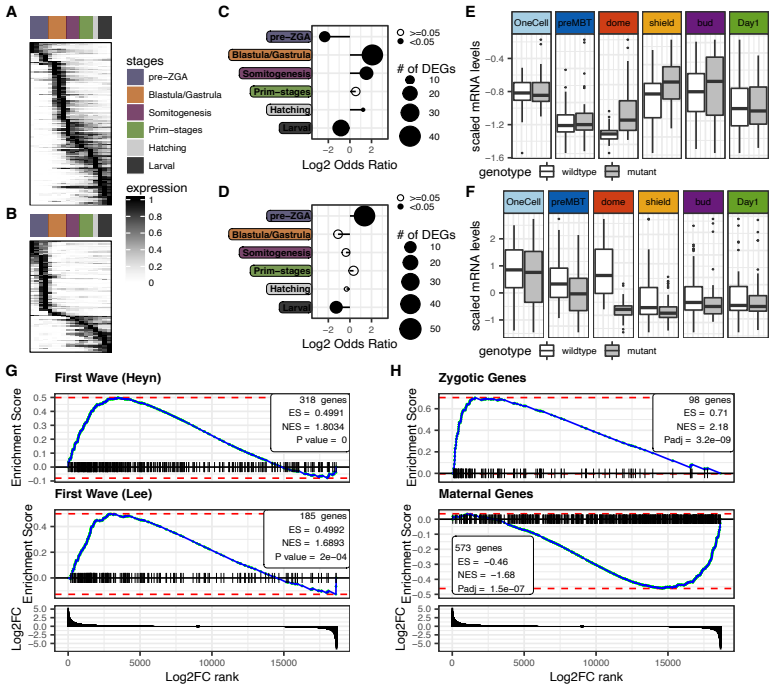

Fig. 6. ZGA transcribed or degraded mRNAs are deregulated in *rif1* mutants. (A-B) Heat plots showing the expression (tags per million scaled to maximum) of *rif1* mutant Dome Up (A) or Down (B) DEGs (rows) across 18 developmental timepoints (columns) in wild type embryos. Expression data is from White, et al. [1]. The legend across the top of each heat plot denotes six developmental phases. (C-D) Log2 odds ratios from Fisher’s exact tests of associations between dome Up (C) or Down (D) DEGs and the developmental phases in A and B. The total number of each DEG expressed in each phase is indicated by the size of the point, and point fills indicate statistical significance. Dome Up or Down DEGs are overrepresented in the Blastula/Gastrula or pre-ZGA phases, respectively. (E-F) Scaled QuantSeq counts for dome Up (E) or Down (F) DEGs across all developmental stages. Overall, dome Up or Down DEGs are normally up- or down-regulated by shield stage, so normal expression of dome DEGs is generally restored by shield. (G) Gene set enrichment analysis showing that genes known to be expressed during the first waves of zebrafish transcription are overexpressed upon Rif1 loss. The genes are ranked by Log2FC in expression between dome stage wild type and *rif1*$^{omf201/omf201}$ embryos, as measured by QuantSeq. (H) Gene set enrichment analysis showing that genes, which are strictly zygotic or maternal, are often up- or down-regulated at dome stage in *rif1* mutants, respectively.

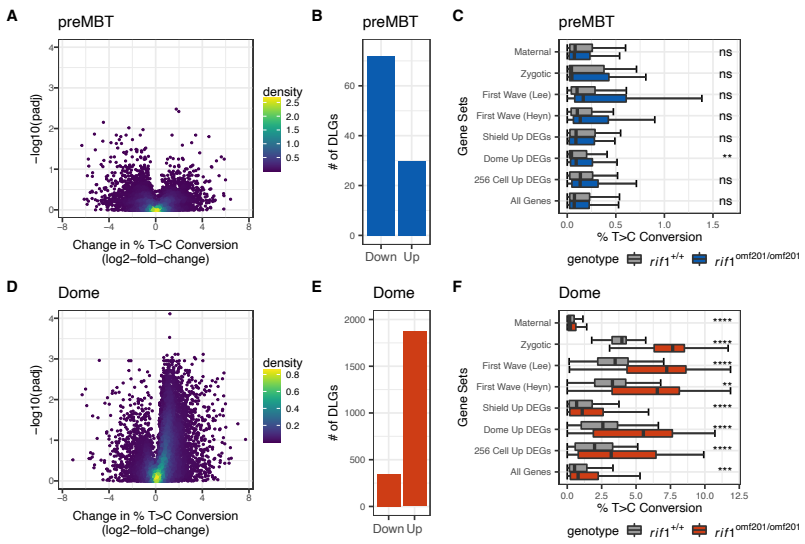

Fig. 7. Labeling of nascent mRNAs reveals that the role for Rif1 in regulating ZGA transcription is pervasive. (A, D) Volcano plots showing the Log2-fold change in T-to-C conversions from SLAM-seq for each transcript between wild type and *rif1* mutant embryos at preMBT (A) or dome (D) stage. P values were calculated using the beta-binomial test and were corrected using the Benjamini & Hochberg method. The colors represent the density of overlapping data points. (B, E). Barplots of the number of differentially labeled genes (DLGs; >1.5-fold change in T-to-C conversions and BH-adjusted p value <= 0.1) in A or D. (C, F) Boxplots of T-to-C conversion percentages at preMBT (C) or dome (F) stage for the following: all genes; DEGs upregulated in *rif1* mutants from this study (256 Cell Up, Dome Up, or Shield Up), genes transcribed during the first ZGA wave from Heyn et al. or Lee et al., or genes identified by Harvey et al. as maternal or zygotic [2-4].

at higher levels (72/98 Log2FC > 0) in mutant embryos at the dome stage compared to wild-type, and most of the zygotic genes were towards the top of the list of genes ranked by dome Log2FC (Fig. 6H top). In contrast, genes in the maternal set were often down in the mutants at dome and were found towards the bottom of the ranked gene list (Fig. 6H bottom). Altogether our data suggest that Rif1 loss enhances the destruction of maternal mRNAs and stimulates the expression of genes during zygotic genome activation.

To directly assess transcription during ZGA, we labeled nascent mRNAs in early embryos with 4-Thiouridine (S4U)(Herzog et al. 2017). By injecting the label into one-cell stage embryos we were able to identify mRNAs synthesized by the pre-MBT (2.5 hours) or dome (4.3 hours) stages. The incorporated label was mapped to mRNAs using thiol(SH)-linked alkylation for metabolic sequencing of RNA (SLAM-seq). SLAM-seq introduces T-to-C conversions at the sites of the incorporated S4U. Thus, each gene's percentage of T-to-C conversions indicates the amount of its mRNA synthesized during the labeling period (zygotic) relative to pre-existing mRNA (maternal).

330 At the pre-MBT stage, there was very little difference in T-to-C conversion percentages
331 between wild-type and *rif1*$^{omf201/omf201}$ mutant embryos, and there were only 102 differentially
332 labeled genes (DLGs) at preMBT (Fig. 7A-C; fold-change in T-to-C conversion > 1.5 and beta-
333 binomial test FDR > 0.1). Therefore, we conclude that zygotic genome activation is not
334 occurring earlier than the MBT for most genes in the *rif1*$^{omf201/omf201}$ mutants. In contrast, there
335 were 1,872 DLGs with increased labeling in mutants at dome (Fig. 7D, E; fold-change in T-to-C
336 conversion > 1.5 and beta-binomial test FDR > 0.1). Furthermore, the T-to-C conversion rates at
337 the dome stage were higher in the *rif1*$^{omf201/omf201}$ mutants for all gene categories analyzed (Fig.
338 7F). The differences in T-to-C conversion were greatest for the genes we previously identified
339 as being overexpressed in the mutants (256-Cell and dome Up-DEGs) and for the genes known
340 to be transcribed during ZGA (First Wave and Zygotic). Notably, we detected a significant
341 difference in mean T-to-C conversion calculated for all labeled genes. Overall, these data
342 demonstrate that Rif1 has pervasive effects on transcription during zygotic genome activation.
343

344 **DISCUSSION**

345 Previous studies of Rif1 in vertebrates have mainly been limited to cell culture models
346 and have not addressed how its loss impacts RT establishment and change in the early embryo.
347 We have developed a zebrafish model to study the developmental effects of Rif1 loss. Using
348 this model, we have determined the impacts of Rif1 knockout on zebrafish embryonic
349 development and survival, RT, and gene expression.

350 Our work adds to our understanding of the importance of Rif1 for vertebrate
351 development. The extent to which Rif1 is essential for embryogenesis has been unclear. In
352 Drosophila melanogaster, Rif1 knockdown by RNA interference caused embryonic lethality, but
353 its knockout by CRISPR-Cas9 caused only mild effects on hatching rates[19, 23, 38]. Rif1
354 knockout phenotypes in mice depend on genetic background and sex. Rif1 is essential in
355 female mice, which die between the blastula and early gastrula stages[27]. Male mice are less

356 affected by Rif1 loss. Although most Rif1 mutant male mice die around mid-gestation, a fraction
357 survives to sexual maturity[25-28]. We observed only mild *rif1* phenotypes during embryonic
358 development. Rif1 loss only slightly delayed epiboly completion. The reason for that delay is
359 unknown, but it may be due to the transcriptional effects of Rif1 loss at the ZGA. The *rif1*
360 mutants also showed a deficiency in primitive hematopoiesis. The first wave of hematopoiesis is
361 not essential for zebrafish development, however it is in mice. Thus, defects in hematopoiesis
362 may contribute to the poor survival of Rif1 mutant mice.

363 The most evident phenotype in the *rif1* mutant zebrafish is the substantial reduction in
364 the number of females. It is tempting to speculate that this phenotype is related to female-
365 specific lethality in mice, but we suspect the underlying causes differ. In part, Rif1 mutant female
366 mice die due to an X chromosome inactivation defect, but zebrafish lack sex chromosomes [27].
367 Furthermore, since we showed that expected numbers of *rif1* mutant fish survive to sexual
368 maturity, the skew in gender ratio must be due to the preferential development of male fish
369 rather than female lethality. A reduction in the proliferation or survival of primordial germ cells
370 (PGCs) causes transdifferentiation of zebrafish to males [39]. To understand how Rif1 promotes
371 female development, we must determine whether its loss affects PGC proliferation. Intriguingly,
372 mouse PGCs exhibit increased replication-transcription conflicts and are sensitive to mutations
373 in Fanconi anemia pathway genes required for replication stress survival[40, 41]. Zebrafish
374 PGCs exhibit high levels of intergenic transcription, which suggests that they may also have
375 increased replication-transcription conflicts[42]. Furthermore, mutations in the Fanconi anemia
376 DNA repair pathway disrupt female zebrafish development[43, 44]. Therefore, the female
377 development defect in the Rif1 mutant zebrafish could be due to deregulated replication fork
378 initiation or impaired replication fork stability in PGCs.

379 Studies with flies and mammalian cells have shown situations where Rif1 becomes less
380 critical for RT once constitutive heterochromatin forms. For example, *D. melanogaster* Rif1
381 delays the replication of specific satellite repeats before H3K9me3 and HP1a associate with

382 them, but once constitutive heterochromatin forms, Rif1 is unnecessary [23, 45]. In human
383 HCT116 cells, late replication of genomic domains with high levels of the heterochromatin mark
384 H3K9me3 does not depend on Rif1 [36]. In contrast, Rif1 knockout nearly completely ablates
385 the RT pattern in human embryonic stem cells, which have relatively little constitutive
386 heterochromatin[36, 46]. Pre-gastrula zebrafish embryos express high levels of Rif1 and
387 substantially lack constitutive heterochromatin [47]. Thus, we were surprised that Rif1 loss had
388 relatively little effect on RT in early embryos. Instead, we found that RT differences were more
389 pronounced later in development. Understanding this paradox will likely reveal mechanisms that
390 control Rif1 activity.

391 Although the effects of Rif1 loss on RT increased as zebrafish development proceeded,
392 the significant developmental changes that shaped the RT profile of late-stage embryos were
393 not affected. For example, *rif1* was not required for the early-to-late timing switches that occur
394 over large segments of chromosomes 4 and 22 during gastrulation, nor was it required for the
395 widespread late-to-early switches that coincided with enhancer activation. Much of the variance
396 in RT between wild-type and mutant embryos was due to a general flattening of the timing
397 profiles, and Rif1 loss did not disrupt the overall peak and valley profile structure. Therefore, our
398 data suggest that instead of causing developmental RT switches in zebrafish, Rif1 sharpens RT
399 caused by other unknown determinants.

400 If Rif1 is not required, what drives developmental changes in RT? Zebrafish embryos
401 establish constitutive heterochromatin by the start of gastrulation, so the early-to-late RT
402 switches that occur during and after that stage might be due to further maturation of
403 heterochromatin[47]. The activation of enhancers might drive late-to-early RT changes
404 throughout the zebrafish genome. Early replicating control elements (ERCEs), which have
405 active epigenetic marks associated with enhancers, cause early replication of large domains in
406 the mouse genome [48]. More work is needed to determine whether the formation of constitutive
407 heterochromatin and activation of ERCEs drive developmental changes in RT in zebrafish.

408 We were particularly interested in whether RT changes in the embryo would lead to
409 transcriptional changes. A long-standing hypothesis is that the RT of a gene can affect its
410 transcriptional competence[49-51]. Recently, Klein et al. used human cell lines in which Rif1
411 could be conditionally depleted to show that its loss caused widespread and coordinated RT
412 and epigenomic changes[36]. Furthermore, the epigenomic alterations caused by Rif1 loss were
413 often associated with gene expression changes[36]. Although this work strongly supports the
414 hypothesis that RT maintains the epigenome, the effects of Rif1 loss in a developing embryo
415 where the RT program and the epigenome are established have not been examined. We used
416 whole-genome RT and RNAseq analysis to determine whether Rif1 loss caused RT changes
417 that led to dysregulated gene expression. Unexpectedly, we found that when Rif1 had the most
418 significant effect on RT during later development, there were few changes in mRNA levels. One
419 limitation of the current work was that we did not directly measure alterations in the epigenome,
420 which may have occurred without transcriptional changes. A second limitation was that we
421 measured RT and gene expression for all cells in the embryo in bulk. Consequently, we were
422 unable to detect cell-to-cell variability in either RT or gene expression. Indeed, RT dysregulation
423 could cause epigenetic variability. Nonetheless, our data show that RT changes caused by Rif1
424 loss do not substantially change overall gene expression later in development.
425 The most pronounced effects of Rif1 loss on transcription were during the earliest stages
426 of development. We previously showed that RT patterns are detected around the MBT in
427 zebrafish embryos, but those patterns are relatively weak compared to later development. In
428 this work, we showed that there was almost no detectable RT pattern in wild-type or Rif1
429 mutants before the ZGA. Despite the lack of RT patterns, Rif1 loss affected the first major wave
430 of transcription. Most genes affected by Rif1 loss at that stage increased slightly, but a
431 significant fraction of all genes transcribed at the ZGA were upregulated. Thus, Rif1 loss had a
432 strong overall effect on transcription at the ZGA.

433 Notably, the role for Rif1 in regulating ZGA transcription is evolutionarily conserved. As
434 we show here for zebrafish, mouse pluripotent cells express Rif1 at high levels, and Rif1
435 expression decreases during cellular differentiation[52]. Multiple groups have reported that Rif1
436 loss in mouse embryonic stem cells (mESCs) causes increased expression of two-cell (2C)
437 zygote-specific genes [35, 53-56]. Given that ZGA occurs through different transcription factors
438 in zebrafish and mice, it is likely that Rif1 affects genes expressed at the ZGA in both species by
439 regulating a common fundamental process rather than the activities of specific transcription
440 factors. mESCs in the 2C state have increased histone marks associated with active
441 transcription, and Rif1 loss is sufficient to cause these chromatin changes [56, 57]. Mouse Rif1
442 co-immunoprecipitates with multiple repressive histone methyltransferases and with the non-
443 canonical polycomb repressive complex PRC1.6, and Rif1 promotes the recruitment of
444 chromatin regulators to several 2C genes in mESCs [57]. We do not know how Rif1 affects the
445 epigenome in the early zebrafish, and this is an important goal for future research. Given the
446 striking similarity in Rif1 function in early zebrafish and mouse embryos, we anticipate the role of
447 Rif1 in regulating transcription in the early embryo will be broadly conserved in vertebrates.
448 In conclusion, we have described multiple phenotypic consequences of Rif1 loss in
449 zebrafish. We found that Rif1 undergoes a functional switch during zebrafish development.
450 When it is highly abundant during early development, Rif1 regulates transcription but does not
451 affect RT. Later in development, Rif1 is important for RT but does not substantially affect gene
452 expression. The zebrafish will be useful for understanding how Rif1 switches between these
453 functional modes at different stages of development. Furthermore, we have identified a new
454 function for Rif1 in sex determination. Thus, the *rif1* mutant zebrafish described here will serve
455 as a valuable model for understanding PGC biology and sex determination.
456

457 **MATERIALS AND METHODS**

458

459 **Animal care.** All animals were handled in strict accordance with protocols approved by
460 the OMRF Institutional Animal Care and Use Committee. Adult breeding fish were housed in an
461 aquatic animal facility in tanks of ~30 fish per tank and maintained at 26.5°C with 10-hour light
462 and 14-hour dark cycles.

463 **TALEN production and microinjection .** The TALEN expression constructs targeting
464 the seventh exon of the *rif1* gene were assembled in pCS2TAL3-DD and pCS2TAL3-RR using
465 Golden Gate Assembly as in Cermak et al. [58]. pCS2TAL3-DD and pCS2TAL3-RR were gifts
466 from David Grunwald (Addgene plasmids # 37275 and 37276; RRID:Addgene_37275;
467 RRID:Addgene_37276). mRNA encoding the TALE nuclease subunits was synthesized using
468 the mMESSAGE mMACHINE SP6 Transcription Kit (AM1340; ThermoFisher Scientific,
469 Waltham, MA) and purified using RNeasy Mini Kit (74104; Qiagen). 125pg of each TALEN
470 mRNA was injected into 1-cell stage zebrafish embryos. TALEN-injected embryos were raised
471 to adulthood and assessed for transmission of insertions/deletions at the TALEN cut site using
472 high resolution melt analysis (HRMA). F1 fish from mutation transmitting F0 animals were raised
473 to adulthood and analyzed for mutation by HRMA, and the specific *rif1* mutation was identified
474 by Sanger sequencing of PCR amplicons spanning the mutation site. *rif1* mutant fish were
475 genotyped using HRMA, Sanger sequencing, and/or competitive allele-specific PCR (KASP
476 assay; LGC).

477 **Zebrafish embryo collection and processing for gDNA, mRNA, or protein.**
478 Zebrafish were spawned as described previously [59]. For QuantSeq, 2-cell embryos were
479 injected with 50 pmoles of 4-Thiouridine (S4U). Embryos were incubated at 28.5°C. Before
480 collection, clutches were visually inspected to ensure that all embryos were developing
481 synchronously. Unfertilized or morphologically abnormal embryos were removed before
482 collection. Whole embryo pools to be used for gDNA or mRNA were rapidly frozen and stored at

483 -80°C for later processing. Embryos were prepared for fluorescence activated cell sorting based
484 on DNA content as described in Siefert et al[59]. Briefly, bud stage or 24 hpf embryos were
485 dechorionated with Pronase, deyolked, and then triturated to a single cell suspension in
486 Phosphate Buffered Saline. Nuclei were prepared from the cells were incubated in DNA staining
487 solution (PBS; 1% Bovine Serum Albumin; 50 ug/ml Propidium iodide P4170-25mg Sigma-
488 Aldrich; 100 ug/ml RNAse A 12091039 Invitrogen) on ice for at least one hour before sorting.
489 The nuclei were then filtered through a 40µm mesh before analysis on a BD LSRII (shield and
490 bud), BD Biosciences FACSAria IIIu (28hpf) or BD Biosciences FACSCalibur. Genomic DNA
491 was prepared from whole embryo pellets or sorted nuclei using the Quick-DNA Miniprep Plus Kit
492 (D4069; Zymo Research). mRNA was prepared from whole embryos using the RNeasy Mini Kit
493 (74104; Qiagen). For protein lysates, whole embryos in pools were deyolked and disaggregated
494 into a single cell suspension as previously described [60], and dry cell pellets were stored at -
495 80°C for later use. To make crude nuclear extract, cell pellets were re-suspended in Buffer A
496 (10mM HEPES, 10mM KCl, 1.5mM $MgCl_2$, 0.34M sucrose, 10% glycerol) with 0.1% triton and
497 protease inhibitors followed by Buffer A plus inhibitors, 0.1% triton and 1uL/mL Benzonase
498 (E1014; Sigma).

499 ***In situ* Hybridization.** The Thisse Lab protocol was followed for the ISH [61]. Briefly,
500 ISH probes were constructed by PCR from genomic DNA and isothermal assembly into HindIII-
501 BamHI digested pUC57-Amp plasmids flanked by T3 and T7 promoters for sense (coding RNA)
502 and anti-sense strand synthesis, respectively. Primers used to amplify probe sequences are as
503 follows: *β-globin* forward acc ctc act aaa ggg aaC GCG CAG CGA TTC AGA ACA T, *β-globin*
504 reverse acg act cac tat agg gcC TTC TGA GGG CTG ACA CAA CA, *gata1a* forward acc ctc act
505 aaa ggg aaA CTC CTC TGA GCC TTC TCG T, and *gata1a* reverse acg act cac tat agg gcT
506 GTG GAG AAG GGC CGT AAA C. Dioxygenin (DIG)-labelled RNA probes were synthesized
507 with T3 and T7 polymerase with reagents from Roche. Embryos were dechorionated with
508 forceps and fixed in 4% paraformaldehyde in 1X PBS overnight. Fixed embryos were

509 dehydrated in 100% methanol and stored at -20°C. The 24 hpf embryos were proteinase K
510 treated for 10 minutes. The protocol was programmed into an Intavis VSi machine to automate
511 the prehybridization and washing procedures. Embryos were removed from the machine and
512 incubated in DIG-labelled RNA probes overnight in a 70°C water bath. Embryos were then
513 returned to the machine for washing, pre-incubation with Bovine Serum Albumin, incubation with
514 anti-DIG antibody, and additional washing. Labelled embryos were imaged with a Nikon
515 SMZ1500 stereomicroscope with Andor Zyla sCMOS camera.

516 **Antibodies used for immunoblotting.** Anti-zebrafish Rif1 antibodies were made by
517 immunizing rabbits with bacterially expressed purified fragments of zebrafish Rif1
518 (NP_001074275.1 amino acids 1-150 or 2199-2347) and were affinity purified from whole serum
519 (Cocalico Biologicals, Inc.). Rabbit polyclonal anti-human Smc3 was a gift from Susannah
520 Rankin [62]. Peroxidase AffiniPure Goat Anti-Rabbit IgG (H+L) was purchased from Jackson
521 Immuno Research Laboratories (RRID: AB_2313567).

522 **Quantitative RT-PCR**. mRNA was converted to cDNA using the AccuScript High
523 Fidelity Reverse Transcriptase (600089; Agilent, Santa Clara, CA). qPCR was done on a
524 LightCycler 480 with the SYBR Green I Master (04707516001; Roche) master mix. Three
525 technical replicates were performed for each sample. The relative mRNA expression was
526 calculated using the $2^{-\Delta\Delta Cq}$ method. The following primer sequences were used: *rif1* forward
527 ACT GGC TGA TGA CAT TGA TCG T, reverse ATC CAG GGC TAC GGA GGT TA; *eef1a1l1*
528 forward CTG GAG GCC AGC TCA AAC AT, reverse ATC AAG AAG AGT AGT ACC GCT AGC
529 ATT AC.

530 **Next generation library preparation and sequencing.** For whole-genome
531 sequencing, 50ng - 2µg of gDNA was sheared to approximately 300 bp fragments using a
532 sonicator (Covaris). The gDNA libraries were prepared using the KAPA Hyper Prep Kit (Roche)
533 with SeqCap (Roche) or Illumina TruSeq (Illumina) adapters. Genomic DNA libraries were
534 sequenced in 150bp paired-end read fragments on an Illumina HiSeq 2500 or NovaSeq 6000.

535 Before library preparation, the SlamSeq mRNA was Iodoacetamide treated using the SLAMseq
536 Kinetics Kit – Anabolic Kinetics Module (Lexogen). The QuantSeq and SlamSeq libraries were
537 prepared using the QuantSeq 3' mRNA-Seq Library Prep Kit for Illumina (Lexogen). RNA
538 sequencing was performed using custom primers on an Illumina Nextseq 500 with High Output
539 chemistry and 75bp single-ended reads.

540 **Replication timing analysis.** RT data were generated based on copy-number
541 variations between filtered G1 and S-phase whole-genome sequencing read counts, as
542 described previously (Siefert, 2017). Pools of >100 whole embryos at preMBT, dome, or shield
543 stage were treated as S-phase samples, since a high percentage cells at these stages are in S
544 phase. Nuclei from bud or 24 hpf embryos were sorted based on DNA content to isolate G1 and
545 S-phase fractions. The data was processed using our RepliTimer pipeline
546 (https://github.com/SansamLab/RepliTimer/tree/v1.0.11; DOI 10.5281/zenodo.6426313.) [63].
547 Whole genome sequencing reads were trimmed with fastp, aligned to the zebrafish genome
548 (GRCz11) using BWA-MEM, and duplicate reads were marked with Picard MarkDuplicates.
549 Properly-paired and non-duplicated reads with MapQ scores of at least 20 were filtered with
550 Bamtools. Alignments were read into GenomicRanges for downstream analysis in R. Reads
551 were also removed if they were within a set of 100 bp windows with anomalously high read
552 counts (exceeding 1.5 times the interquartile range in at least 4 out of 65 whole genome
553 sequencing runs from this study and previously published work)[30]. Genomic windows for
554 calculating RT were defined as regions with a minimum of 400 reads in every sample. An S/G1
555 quotient was calculated for each window, and quotients were smoothed and Log2 transformed
556 [30].

557 **RNA sequencing analysis (QuantSeq 3' mRNA-Seq and SLAM-Seq).** The QuantSeq
558 data was analyzed using our QuantSeqPipeline pipeline (https://github.com/SansamLab-
559 Pipelines-Genomics/QuantSeqPipeline/releases/tag/v0.1.2; DOI 10.5281/zenodo.6622164).
560 Reads were trimmed with bbmap and aligned to GRCz11 with STAR. Using a custom R script,

probable internal priming sites at polyA genomic sequences were identified and reads mapping to those sites were removed. Reads aligning to 3' ends of transcripts are then counted. The 4.3.2 transcript annotation by Lawson et al was used [64]. Differentially expressed genes were identified using DESeq2, and plots were generated in R. The SLAM-Seq sequencing reads were aligned and T-to-C conversion rates were calculated using the SLAM-DUNK package with default settings [65].

ACKNOWLEDGEMENTS

This work was supported by National Institutes of Health National Institute of General Medical Sciences grant 1R01GM121703 and by the Oklahoma Center for Adult Stem Cell Research.

COMPETING INTERESTS

No competing interests declared.

AUTHOR CONTRIBUTIONS

cls, eam, jcs, and tdn conceived and designed the experiments and analysis. jcs generated the *rif1* mutant. eam, tdn, and cgs performed the RT experiments. jcs performed the in situ hybridizations. eam performed the RNASeq and SlamSeq experiments. eam performed the live embryo imaging and qRT-PCR analysis. eam and dg performed the large cohort genotyping experiments. eam, dg, cgs, and tdn raised breeding cohorts for the majority of experiments. cls, eam, and tdn analyzed the RT, RNASeq, and SlamSeq data. cls, eam, and tdn wrote the paper.

583 **REFERENCES**

584 1. White RJ, Collins JE, Sealy IM, Wali N, Dooley CM, Digby Z, et al. A high-resolution
585 mRNA expression time course of embryonic development in zebrafish. Elife. 2017;6. Epub
586 20171116. doi: 10.7554/eLife.30860. PubMed PMID: 29144233; PubMed Central PMCID:
587 PMCPMC5690287.
588 2. Heyn P, Kircher M, Dahl A, Kelso J, Tomancak P, Kalinka AT, et al. The earliest
589 transcribed zygotic genes are short, newly evolved, and different across species. Cell Rep.
590 2014;6(2):285-92. Epub 20140116. doi: 10.1016/j.celrep.2013.12.030. PubMed PMID:
591 24440719.
592 3. Lee MT, Bonneau AR, Takacs CM, Bazzini AA, DiVito KR, Fleming ES, et al. Nanog,
593 Pou5f1 and SoxB1 activate zygotic gene expression during the maternal-to-zygotic transition.
594 Nature. 2013;503(7476):360-4. Epub 20130922. doi: 10.1038/nature12632. PubMed PMID:
595 24056933; PubMed Central PMCID: PMCPMC3925760.
596 4. Harvey SA, Sealy I, Kettleborough R, Fenyes F, White R, Stemple D, et al. Identification
597 of the zebrafish maternal and paternal transcriptomes. Development. 2013;140(13):2703-10.
598 Epub 20130529. doi: 10.1242/dev.095091. PubMed PMID: 23720042; PubMed Central PMCID:
599 PMCPMC3678340.
600 5. Rhind N, Gilbert DM. DNA replication timing. Cold Spring Harb Perspect Biol.
601 2013;5(8):a010132. Epub 20130801. doi: 10.1101/cshperspect.a010132. PubMed PMID:
602 23838440; PubMed Central PMCID: PMCPMC3721284.
603 6. Hiratani I, Ryba T, Itoh M, Rathjen J, Kulik M, Papp B, et al. Genome-wide dynamics of
604 replication timing revealed by in vitro models of mouse embryogenesis. Genome Res.
605 2010;20(2):155-69. Epub 20091201. doi: 10.1101/gr.099796.109. PubMed PMID: 19952138;
606 PubMed Central PMCID: PMCPMC2813472.
607 7. Hiratani I, Ryba T, Itoh M, Yokochi T, Schwaiger M, Chang CW, et al. Global
608 reorganization of replication domains during embryonic stem cell differentiation. PLoS Biol.
609 2008;6(10):e245. doi: 10.1371/journal.pbio.0060245. PubMed PMID: 18842067; PubMed
610 Central PMCID: PMCPMC2561079.
611 8. MacAlpine DM, Rodríguez HK, Bell SP. Coordination of replication and transcription
612 along a Drosophila chromosome. Genes Dev. 2004;18(24):3094-105. doi:
613 10.1101/gad.1246404. PubMed PMID: 15601823; PubMed Central PMCID: PMCPMC535919.
614 9. White EJ, Emanuelsson O, Scalzo D, Royce T, Kosak S, Oakeley EJ, et al. DNA
615 replication-timing analysis of human chromosome 22 at high resolution and different
616 developmental states. Proc Natl Acad Sci U S A. 2004;101(51):17771-6. Epub 20041210. doi:
617 10.1073/pnas.0408170101. PubMed PMID: 15591350; PubMed Central PMCID:
618 PMCPMC539744.
619 10. Schübeler D, Scalzo D, Kooperberg C, van Steensel B, Delrow J, Groudine M. Genome-
620 wide DNA replication profile for Drosophila melanogaster: a link between transcription and
621 replication timing. Nat Genet. 2002;32(3):438-42. Epub 20020930. doi: 10.1038/ng1005.
622 PubMed PMID: 12355067.
623 11. Dixon JR, Jung I, Selvaraj S, Shen Y, Antosiewicz-Bourget JE, Lee AY, et al. Chromatin
624 architecture reorganization during stem cell differentiation. Nature. 2015;518(7539):331-6. doi:
625 10.1038/nature14222. PubMed PMID: 25693564; PubMed Central PMCID: PMCPMC4515363.
626 12. Zhou J, Ermakova OV, Riblet R, Birshtein BK, Schildkraut CL. Replication and
627 subnuclear location dynamics of the immunoglobulin heavy-chain locus in B-lineage cells. Mol
628 Cell Biol. 2002;22(13):4876-89. doi: 10.1128/mcb.22.13.4876-4889.2002. PubMed PMID:
629 12052893; PubMed Central PMCID: PMCPMC133899.
630 13. Cornacchia D, Dileep V, Quivy JP, Foti R, Tili F, Santarella-Mellwig R, et al. Mouse Rif1
631 is a key regulator of the replication-timing programme in mammalian cells. EMBO J.

632 2012;31(18):3678-90. doi: 10.1038/emboj.2012.214. PubMed PMID: 22850673; PubMed
633 Central PMCID: PMCPMC3442270.
634 14. Hayano M, Kanoh Y, Matsumoto S, Renard-Guillet C, Shirahige K, Masai H. Rif1 is a
635 global regulator of timing of replication origin firing in fission yeast. Genes Dev. 2012;26(2):137-
636 50. Epub 2012/01/27. doi: 10.1101/gad.178491.111. PubMed PMID: 22279046; PubMed
637 Central PMCID: PMCPMC3273838.
638 15. Hiraga S, Alvino GM, Chang F, Lian HY, Sridhar A, Kubota T, et al. Rif1 controls DNA
639 replication by directing Protein Phosphatase 1 to reverse Cdc7-mediated phosphorylation of the
640 MCM complex. Genes Dev. 2014;28(4):372-83. Epub 2014/02/18. doi:
641 10.1101/gad.231258.113. PubMed PMID: 24532715; PubMed Central PMCID:
642 PMCPMC3937515.
643 16. Yamazaki S, Ishii A, Kanoh Y, Oda M, Nishito Y, Masai H. Rif1 regulates the replication
644 timing domains on the human genome. EMBO J. 2012;31(18):3667-77. doi:
645 10.1038/emboj.2012.180. PubMed PMID: 22850674; PubMed Central PMCID:
646 PMCPMC3442267.
647 17. Davé A, Cooley C, Garg M, Bianchi A. Protein phosphatase 1 recruitment by Rif1
648 regulates DNA replication origin firing by counteracting DDK activity. Cell Rep. 2014;7(1):53-61.
649 Epub 2014/03/25. doi: 10.1016/j.celrep.2014.02.019. PubMed PMID: 24656819; PubMed
650 Central PMCID: PMCPMC3989773.
651 18. Mattarocci S, Shyian M, Lemmens L, Damay P, Altintas DM, Shi T, et al. Rif1 controls
652 DNA replication timing in yeast through the PP1 phosphatase Glc7. Cell Rep. 2014;7(1):62-9.
653 Epub 2014/04/02. doi: 10.1016/j.celrep.2014.03.010. PubMed PMID: 24685139.
654 19. Sreesankar E, Bharathi V, Mishra RK, Mishra K. Drosophila Rif1 is an essential gene
655 and controls late developmental events by direct interaction with PP1-87B. Sci Rep.
656 2015;5:10679. Epub 2015/05/30. doi: 10.1038/srep10679. PubMed PMID: 26022086; PubMed
657 Central PMCID: PMCPMC4448129.
658 20. Sukackaite R, Cornacchia D, Jensen MR, Mas PJ, Blackledge M, Enervald E, et al.
659 Mouse Rif1 is a regulatory subunit of protein phosphatase 1 (PP1). Sci Rep. 2017;7(1):2119.
660 Epub 2017/05/20. doi: 10.1038/s41598-017-01910-1. PubMed PMID: 28522851; PubMed
661 Central PMCID: PMCPMC5437018.
662 21. Foti R, Gnan S, Cornacchia D, Dileep V, Bulut-Karslioglu A, Diehl S, et al. Nuclear
663 Architecture Organized by Rif1 Underpins the Replication-Timing Program. Mol Cell.
664 2016;61(2):260-73. Epub 20151224. doi: 10.1016/j.molcel.2015.12.001. PubMed PMID:
665 26725008; PubMed Central PMCID: PMCPMC4724237.
666 22. Hiraga SI, Ly T, Garzón J, Hořejší Z, Ohkubo YN, Endo A, et al. Human RIF1 and
667 protein phosphatase 1 stimulate DNA replication origin licensing but suppress origin activation.
668 EMBO Rep. 2017;18(3):403-19. Epub 2017/01/13. doi: 10.15252/embr.201641983. PubMed
669 PMID: 28077461; PubMed Central PMCID: PMCPMC5331243.
670 23. Seller CA, O'Farrell PH. Rif1 prolongs the embryonic S phase at the Drosophila mid-
671 blastula transition. PLoS Biol. 2018;16(5):e2005687. Epub 2018/05/11. doi:
672 10.1371/journal.pbio.2005687. PubMed PMID: 29746464; PubMed Central PMCID:
673 PMCPMC5963817.
674 24. Meléndez García R, Haccard O, Chesneau A, Narassimprakash H, Roger J, Perron M,
675 et al. A non-transcriptional function of Yap regulates the DNA replication program in Xenopus
676 laevis. eLife. 2022;11:e75741. doi: 10.7554/eLife.75741.
677 25. Chapman JR, Barral P, Vannier JB, Borel V, Steger M, Tomas-Loba A, et al. RIF1 is
678 essential for 53BP1-dependent nonhomologous end joining and suppression of DNA double-
679 strand break resection. Mol Cell. 2013;49(5):858-71. Epub 2013/01/22. doi:
680 10.1016/j.molcel.2013.01.002. PubMed PMID: 23333305; PubMed Central PMCID:
681 PMCPMC3594748.

682 26. Daxinger L, Harten SK, Oey H, Epp T, Isbel L, Huang E, et al. An ENU mutagenesis
683 screen identifies novel and known genes involved in epigenetic processes in the mouse.
684 Genome Biol. 2013;14(9):R96. Epub 2013/09/13. doi: 10.1186/gb-2013-14-9-r96. PubMed
685 PMID: 24025402; PubMed Central PMCID: PMCPMC4053835.
686 27. Enervald E, Powell LM, Boteva L, Foti R, Blanes Ruiz N, Kibar G, et al. RIF1 and KAP1
687 differentially regulate the choice of inactive versus active X chromosomes. Embo j.
688 2021;40(24):e105862. Epub 20211117. doi: 10.15252/embj.2020105862. PubMed PMID:
689 34786738; PubMed Central PMCID: PMCPMC8672179.
690 28. Buonomo SB, Wu Y, Ferguson D, de Lange T. Mammalian Rif1 contributes to replication
691 stress survival and homology-directed repair. J Cell Biol. 2009;187(3):385-98. doi:
692 10.1083/jcb.200902039. PubMed PMID: 19948482; PubMed Central PMCID:
693 PMCPMC2779251.
694 29. Ho RK, Kimmel CB. Commitment of cell fate in the early zebrafish embryo. Science.
695 1993;261(5117):109-11. doi: 10.1126/science.8316841. PubMed PMID: 8316841.
696 30. Siefert JC, Georgescu C, Wren JD, Koren A, Sansam CL. DNA replication timing during
697 development anticipates transcriptional programs and parallels enhancer activation. Genome
698 Res. 2017;27(8):1406-16. doi: 10.1101/gr.218602.116. PubMed PMID: 28512193; PubMed
699 Central PMCID: PMCPMC5538556.
700 31. Alavi S, Ghadiri H, Dabirmanesh B, Moriyama K, Khajeh K, Masai H. G-quadruplex
701 binding protein Rif1, a key regulator of replication timing. J Biochem. 2021;169(1):1-14. doi:
702 10.1093/jb/mvaa128. PubMed PMID: 33169133.
703 32. Kimmel CB, Ballard WW, Kimmel SR, Ullmann B, Schilling TF. Stages of embryonic
704 development of the zebrafish. Dev Dyn. 1995;203(3):253-310. doi: 10.1002/aja.1002030302.
705 PubMed PMID: 8589427.
706 33. Kossack ME, Draper BW. Genetic regulation of sex determination and maintenance in
707 zebrafish (Danio rerio). Curr Top Dev Biol. 2019;134:119-49. Epub 20190321. doi:
708 10.1016/bs.ctdb.2019.02.004. PubMed PMID: 30999973; PubMed Central PMCID:
709 PMCPMC6894417.
710 34. Bogdanovic O, Fernandez-Miñán A, Tena JJ, de la Calle-Mustienes E, Hidalgo C, van
711 Kruysbergen I, et al. Dynamics of enhancer chromatin signatures mark the transition from
712 pluripotency to cell specification during embryogenesis. Genome Res. 2012;22(10):2043-53.
713 Epub 20120516. doi: 10.1101/gr.134833.111. PubMed PMID: 22593555; PubMed Central
714 PMCID: PMCPMC3460198.
715 35. Dan J, Liu Y, Liu N, Chiourea M, Okuka M, Wu T, et al. Rif1 maintains telomere length
716 homeostasis of ESCs by mediating heterochromatin silencing. Developmental cell.
717 2014;29(1):7-19.
718 36. Klein KN, Zhao PA, Lyu X, Sasaki T, Bartlett DA, Singh AM, et al. Replication timing
719 maintains the global epigenetic state in human cells. Science. 2021;372(6540):371-8. Epub
720 2021/04/24. doi: 10.1126/science.aba5545. PubMed PMID: 33888635; PubMed Central PMCID:
721 PMCPMC8173839.
722 37. Giraldez AJ, Mishima Y, Rihel J, Grocock RJ, Van Dongen S, Inoue K, et al. Zebrafish
723 MiR-430 promotes deadenylation and clearance of maternal mRNAs. Science.
724 2006;312(5770):75-9. Epub 20060216. doi: 10.1126/science.1122689. PubMed PMID:
725 16484454.
726 38. Armstrong RL, Das S, Hill CA, Duronio RJ, Nordman JT. Rif1 Functions in a Tissue-
727 Specific Manner To Control Replication Timing Through Its PP1-Binding Motif. Genetics.
728 2020;215(1):75-87. Epub 20200306. doi: 10.1534/genetics.120.303155. PubMed PMID:
729 32144132; PubMed Central PMCID: PMCPMC7198277.
730 39. Tzung K-W, Goto R, Saju JM, Sreenivasan R, Saito T, Arai K, et al. Early depletion of
731 primordial germ cells in zebrafish promotes testis formation. Stem cell reports. 2015;4(1):61-73.

40. Luo Y, Hartford SA, Zeng R, Southard TL, Shima N, Schimenti JC. Hypersensitivity of primordial germ cells to compromised replication-associated DNA repair involves ATM-p53-p21 signaling. PLoS Genet. 2014;10(7):e1004471. Epub 20140710. doi: 10.1371/journal.pgen.1004471. PubMed PMID: 25010009; PubMed Central PMCID: PMCPMC4091704.
41. Yang Y, Xu W, Gao F, Wen C, Zhao S, Yu Y, et al. Transcription-replication conflicts in primordial germ cells necessitate the Fanconi anemia pathway to safeguard genome stability. Proc Natl Acad Sci U S A. 2022;119(34):e2203208119. Epub 20220815. doi: 10.1073/pnas.2203208119. PubMed PMID: 35969748; PubMed Central PMCID: PMCPMC9407672.
42. Redl S, de Jesus Domingues AM, Caspani E, Möckel S, Salvenmoser W, Mendez-Lago M, et al. Extensive nuclear gyration and pervasive non-genic transcription during primordial germ cell development in zebrafish. Development. 2021;148(2). Epub 20210120. doi: 10.1242/dev.193060. PubMed PMID: 33298460; PubMed Central PMCID: PMCPMC7847270.
43. Rodríguez-Marí A, Cañestro C, Bremiller RA, Nguyen-Johnson A, Asakawa K, Kawakami K, et al. Sex reversal in zebrafish fancl mutants is caused by Tp53-mediated germ cell apoptosis. PLoS Genet. 2010;6(7):e1001034. Epub 20100722. doi: 10.1371/journal.pgen.1001034. PubMed PMID: 20661450; PubMed Central PMCID: PMCPMC2908690.
44. Ramanagoudr-Bhojappa R, Carrington B, Ramaswami M, Bishop K, Robbins GM, Jones M, et al. Multiplexed CRISPR/Cas9-mediated knockout of 19 Fanconi anemia pathway genes in zebrafish revealed their roles in growth, sexual development and fertility. PLoS Genet. 2018;14(12):e1007821. Epub 20181212. doi: 10.1371/journal.pgen.1007821. PubMed PMID: 30540754; PubMed Central PMCID: PMCPMC6328202.
45. Yuan K, O'Farrell PH. TALE-light imaging reveals maternally guided, H3K9me2/3-independent emergence of functional heterochromatin in Drosophila embryos. Genes Dev. 2016;30(5):579-93. Epub 20160225. doi: 10.1101/gad.272237.115. PubMed PMID: 26915820; PubMed Central PMCID: PMCPMC4782051.
46. Hawkins RD, Hon GC, Lee LK, Ngo Q, Lister R, Pelizzola M, et al. Distinct epigenomic landscapes of pluripotent and lineage-committed human cells. Cell Stem Cell. 2010;6(5):479-91. doi: 10.1016/j.stem.2010.03.018. PubMed PMID: 20452322; PubMed Central PMCID: PMCPMC2867844.
47. Laue K, Rajshekar S, Courtney AJ, Lewis ZA, Goll MG. The maternal to zygotic transition regulates genome-wide heterochromatin establishment in the zebrafish embryo. Nat Commun. 2019;10(1):1551. Epub 2019/04/06. doi: 10.1038/s41467-019-09582-3. PubMed PMID: 30948728; PubMed Central PMCID: PMCPMC6449393.
48. Sima J, Chakraborty A, Dileep V, Michalski M, Klein KN, Holcomb NP, et al. Identifying cis Elements for Spatiotemporal Control of Mammalian DNA Replication. Cell. 2019;176(4):816-30.e18. Epub 20181227. doi: 10.1016/j.cell.2018.11.036. PubMed PMID: 30595451; PubMed Central PMCID: PMCPMC6546437.
49. Gottesfeld J, Bloomer LS. Assembly of transcriptionally active 5S RNA gene chromatin in vitro. Cell. 1982;28(4):781-91. Epub 1982/04/01. doi: 10.1016/0092-8674(82)90057-5. PubMed PMID: 7201351.
50. Lande-Diner L, Zhang J, Cedar H. Shifts in replication timing actively affect histone acetylation during nucleosome reassembly. Mol Cell. 2009;34(6):767-74. doi: 10.1016/j.molcel.2009.05.027. PubMed PMID: 19560427; PubMed Central PMCID: PMCPMC2717743.
51. Zhang J, Xu F, Hashimshony T, Keshet I, Cedar H. Establishment of transcriptional competence in early and late S phase. Nature. 2002;420(6912):198-202. Epub 2002/11/15. doi: 10.1038/nature01150. PubMed PMID: 12432398.

52. Adams IR, McLaren A. Identification and characterisation of mRif1: A mouse telomere-associated protein highly expressed in germ cells and embryo-derived pluripotent stem cells. Developmental Dynamics: An Official Publication of the American Association of Anatomists. 2004;229(4):733-44.
53. Li P, Wang L, Bennett BD, Wang J, Li J, Qin Y, et al. Rif1 promotes a repressive chromatin state to safeguard against endogenous retrovirus activation. Nucleic acids research. 2017;45(22):12723-38.
54. Li L, Li P, Chen J, Li L, Shen Y, Zhu Y, et al. Rif1 interacts with non-canonical polycomb repressive complex PRC1.6 to regulate mouse embryonic stem cells fate potential. Cell Regen. 2022;11(1):25. Epub 20220802. doi: 10.1186/s13619-022-00124-9. PubMed PMID: 35915272; PubMed Central PMCID: PMCPMC9343540.
55. Zhang W, Yao C, Luo Y, Li Q, Zhao Q, Zhao Y, et al. Rif1 and Hmgn3 regulate the conversion of murine trophoblast stem cells. Cell Rep. 2022;38(13):110570. doi: 10.1016/j.celrep.2022.110570. PubMed PMID: 35354046.
56. Yoshizawa-Sugata N, Yamazaki S, Mita-Yoshida K, Ono T, Nishito Y, Masai H. Loss of full-length DNA replication regulator Rif1 in two-cell embryos is associated with zygotic transcriptional activation. Journal of Biological Chemistry. 2021;297(6):101367. doi: https://doi.org/10.1016/j.jbc.2021.101367.
57. Li P, Wang L, Bennett BD, Wang J, Li J, Qin Y, et al. Rif1 promotes a repressive chromatin state to safeguard against endogenous retrovirus activation. Nucleic Acids Res. 2017;45(22):12723-38. Epub 2017/10/19. doi: 10.1093/nar/gkx884. PubMed PMID: 29040764; PubMed Central PMCID: PMCPMC5727408.
58. Cermak T, Doyle EL, Christian M, Wang L, Zhang Y, Schmidt C, et al. Efficient design and assembly of custom TALEN and other TAL effector-based constructs for DNA targeting. Nucleic Acids Res. 2011;39(12):e82. Epub 2011/04/16. doi: 10.1093/nar/gkr218. PubMed PMID: 21493687; PubMed Central PMCID: PMCPMC3130291.
59. Siefert JC, Clowdus EA, Goins D, Koren A, Sansam CL. Profiling DNA Replication Timing Using Zebrafish as an In Vivo Model System. J Vis Exp. 2018;(134). Epub 2018/05/15. doi: 10.3791/57146. PubMed PMID: 29757277; PubMed Central PMCID: PMCPMC6101039.
60. Link V, Carvalho L, Castanon I, Stockinger P, Shevchenko A, Heisenberg CP. Identification of regulators of germ layer morphogenesis using proteomics in zebrafish. J Cell Sci. 2006;119(Pt 10):2073-83. Epub 20060425. doi: 10.1242/jcs.02928. PubMed PMID: 16638810.
61. Thisse C, Thisse B. High-resolution in situ hybridization to whole-mount zebrafish embryos. Nature Protocols. 2008;3(1):59-69. doi: 10.1038/nprot.2007.514.
62. Lafont AL, Song J, Rankin S. Sororin cooperates with the acetyltransferase Eco2 to ensure DNA replication-dependent sister chromatid cohesion. Proceedings of the National Academy of Sciences. 2010;107(47):20364-9. doi: doi:10.1073/pnas.1011069107.
63. Sansam CL. RepliTimer (v1.0.8). 2022.
64. Lawson ND, Li R, Shin M, Grosse A, Yukselen O, Stone OA, et al. An improved zebrafish transcriptome annotation for sensitive and comprehensive detection of cell type-specific genes. eLife. 2020;9:e55792. doi: 10.7554/eLife.55792.
65. Neumann T, Herzog VA, Muhar M, von Haeseler A, Zuber J, Ameres SL, et al. Quantification of experimentally induced nucleotide conversions in high-throughput sequencing datasets. BMC Bioinformatics. 2019;20(1):258. doi: 10.1186/s12859-019-2849-7.